Original scientific paper
https://doi.org/10.33180/InfMIDEM2022.302

Informacije MIDEM
Journal of Microelectronics,
Electronic Components and Materials
Vol. 52, No. 3(2022), 159 – 167

Dual-Band X-Shaped Absorber Design for Sensor Applications

Alparslan Cinar[1, 2], S. Cumhur Basaran[2]

[1]Elmali Vocational School, Akdeniz University, Antalya, Turkey
[2]Department of Electrical-Electronics Engineering, Akdeniz University, Antalya, Turkey

Abstract: This study presents a compact absorber design with an X-shaped resonator (XSR) in the S-band region. The proposed design offers single or dual-band absorption peaks, depending on whether the arm lengths of the resonator are symmetrical or asymmetrical. Prototype fabrications of the absorber, whose numerical design was carried out using CST Microwave Studio, were also measured for verification. Based on the simulated and measured results, the proposed absorber exhibited over 93% absorption spectra with relatively narrow bandwidth characteristics desired, especially for sensor applications. It also provided cross-polarized reflections of less than 0.08 at the frequencies of interest. In addition, the absorption frequency changes depending on the dielectric constant and thickness variations of the sensing layer placed on the absorber were obtained numerically and experimentally to investigate the sensing performance of a dual-band configuration of the absorber. In addition, the same analyzes and measurements were carried out again for two separate single-band split-ring resonator (SRR)-based absorbers designed in this study, and their sensing performances were compared with the dual-band X-shaped absorber's (XSA) performance. As a result, it was found that the proposed XSA was more sensitive than the SRR-based absorber (SRRA), considering the comparison results.

Keywords: Dual-band absorber; SRR-based absorber; sensor-based absorber; X-shaped absorber

Zasnova dvopasovnega absorberja v obliki X za senzorske aplikacije

Izvleček: Študija predstavlja kompaktno zasnovo absorberja z resonatorjem v obliki črke X (XSR) v območju pasu S. Predlagana zasnova ponuja eno- ali dvopasovne absorpcijske vrhove, odvisno od tega, ali so dolžine rok resonatorja simetrične ali asimetrične. Za preverjanje smo izmerili tudi prototipne izdelave absorberja, katerega numerična zasnova je bila izvedena s programom CST Microwave Studio. Na podlagi simuliranih in izmerjenih rezultatov je predlagani absorber pokazal več kot 93-odstotni absorpcijski spekter z relativno ozko pasovno širino, ki je zaželena zlasti za senzorske aplikacije. Zagotovil je tudi navzkrižno polarizirane odboje, manjše od 0,08 pri želenih frekvencah. Poleg tega so bile numerično in eksperimentalno pridobljene spremembe absorpcijske frekvence v odvisnosti od dielektrične konstante in spremembe debeline senzorske plasti, nameščene na absorber, da bi raziskali senzorsko zmogljivost dvopasovne konfiguracije absorberja. Poleg tega so bile iste analize in meritve ponovno opravljene za dva ločena enopasovna absorberja na osnovi deljenega obročnega resonatorja (SRR), zasnovana v tej študiji, in njune zmogljivosti zaznavanja so bile primerjane z zmogljivostjo dvopasovnega absorberja v obliki črke X (XSA). Na podlagi rezultatov primerjave je bilo ugotovljeno, da je predlagani XSA občutljivejši od absorberja na osnovi SRR (SRRA).

Ključne besede: dvopasovni absorber; absorber na osnovi SRR; absorber na osnovi senzorja; absorber v obliki črke X

** Corresponding Author's e-mail: alparslancinar@akdeniz.edu.tr*

1 Introduction

Resonator-based electromagnetic wave absorbers have been a popular research topic since 2008, when metamaterials were first considered in absorber structures [1]. Thanks to possessing the capability of high absorption rate, resonator-based absorbers are used in a wide variety of applications such as energy harvest [2], amplitude modulation [3], switching [4], stealth technology [5, 6], solar energy [7], and EMI/EMC [8]. One of the application areas where resonator-based absorbers are used extensively is sensors. Sensor-based absorbers are used to detect physical parameters such

How to cite:
A. Cinar et al., "Dual-Band X-Shaped Absorber Design for Sensor Applications", Inf. Midem-J. Microelectron. Electron. Compon. Mater., Vol. 52, No. 3(2022), pp. 159–167

as pressure, temperature, density and determine the electromagnetic properties of materials under test (MUT). In practical applications, they are expected to have physical properties such as ease of manufacture, compactness, reusability, low cost, and electrical properties such as high sensitivity and quality factor. Many absorber designs of various types and specifications that can meet the principal requirements of the sensor applications have been reported in the literature [9-20]. In most of these studies, SRRs have been used as the primary absorbing structure, allowing high selectivity and quality factors due to their inherent resonant characteristic [10-16]. On the other hand, flower-shaped surrounded with the circular ring in [17] and swastika-shaped resonators in [18] have been considered absorbing elements for sensor applications. Similarly, microstructure metamaterial and substrate integrated waveguide cavity resonators have been employed in [19] and [20], respectively.

This study proposes a novel compact absorber design based on an XSR for the S-band frequency region and investigates its sensor performance. Considering the resonator-based absorbers reported in the literature, the most prominent feature of the proposed design is its simple structure consisting of only one resonator placed on a one-layer substrate. Moreover, the proposed design offers to control the transition between single and dual-band absorption characteristics. The XSR on the single top layer is configured such that the central axes of the two arms coincide at the center of the resonator, dividing both arms in half. When the XSR is symmetrical, a single band frequency response is obtained depending on its arm lengths. When an offset is created between the arm lengths, a dual-band frequency response is achieved thanks to this asymmetric structure, and the absorption frequencies of both bands can be tuned by controlling the offset value. The resonator structure with various dimensions has been analyzed, and corresponding absorption characteristics and surface current density at the respective frequencies are presented in this paper. In addition, two different prototypes, symmetrical and non-symmetrical, were fabricated, and then their absorption characteristics were measured to verify the numerical design.

On the other hand, considering the absorption characteristics, the proposed absorber exhibits a relatively narrow bandwidth performance, which is desired especially for sensor applications. In this context, to evaluate the sensor performance of the proposed absorber, the change in the absorption frequency depends on the dielectric constant and thickness variation of a test material placed on the asymmetric absorber structure providing dual-band absorption peaks at 3.12 and 3.52 GHz was investigated. Also, the proposed absorber's sensitivity of frequency shift was compared to two different SRRAs offering single band absorption peaks at 3.12 GHz and 3.52 GHz, respectively, to support the sensor performance. According to the analysis and measurement results, it was observed that the sensitivity of the proposed absorber was higher than the compared absorbers. In addition to the high sensitivity, its simple and compact structure providing dual-band absorption make the proposed design an important candidate that can be used for sensor applications.

2 Numerical design and experimental setup

Schematic views and design parameters of the proposed absorber configuration are depicted in Fig. 1. As seen, the top plate of the absorber is composed of a copper XSR having a thickness of 0.035 mm and an estimated conductivity of 5.8×10^7 S/m. The copper resonator is printed on a Rogers TMM4 substrate having dielectric permittivity (ε_r) of 4.5 and loss tangent (tan δ) of 0.002. The other side of the substrate is fully covered with the same copper material and is set as the ground plane of the absorber. Herein, the volume of Rogers TMM4 substrate is $L_s \times W_s \times h$, where L_s, W_s, and h are 72.136, 34.036, and 0.76 (all in mm), respectively. On the other hand, l_1, l_2, and w stand for design parameters of the XSR structure, as can be seen in Fig. 1. The w value of 4 mm is also fixed in the design.

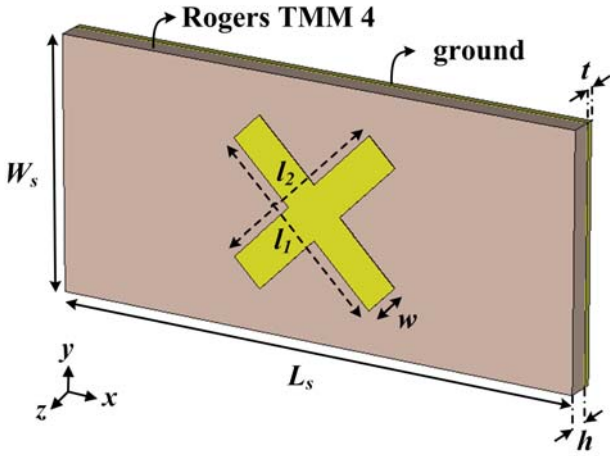

Figure 1: The schematic view and design parameters of the absorber structures.

The absorber's design and numerical analyses were conducted using CST microwave studio (MWS) based on the finite element method. The simulation setup of the absorber is illustrated in Fig. 2(a). Here it is seen that the sidewalls of the waveguide lying on the z-axis are modeled as perfect electrical conductor boundaries ($E_t = 0$). For the excitation purpose, two ends of the waveguide are terminated with input and output ports. Also, the absorber is excited by the TE_{10} mode waveguide

port, where electric field vector *E*, magnetic field vector *H*, and propagation vector *k* are along the *y*, *x* and, *z*-axis, respectively. Four prototypes of different sizes were fabricated and measured to verify the numerical design. The λ/4 spacer with a sample prototype and photographs of the measurement setup are shown in Fig. 2(b) and 2(c), respectively. The reflection and transmission coefficient measurements of each prototype placed in the λ/4 spacer were performed using the S-band WR284 waveguide connected to the Agilent Fieldfox N9926A vector network analyzer.

The relationship between the size of the proposed geometry and the resonant frequency has been explained in formula (1).

$$l = \frac{c}{2f\sqrt{\varepsilon_e}} \tag{1}$$

Where *l* is the length of each XSR's arms, *c* is the speed of light, *f* is operating frequency, and ε_e is the effective permittivity of XSR. And also, the effective permittivity of XSR has been calculated using the following equation:

$$\varepsilon_e = \frac{\varepsilon_r + 1}{2} + \frac{\varepsilon_r - 1}{2}\frac{1}{\sqrt{1+12\frac{h}{w}}} \tag{2}$$

Where ε_r is the dielectric permittivity of the substrate of XSA, *h* is the thickness of the substrate of XSA and *w* is the width of any of XSR's arms [21].

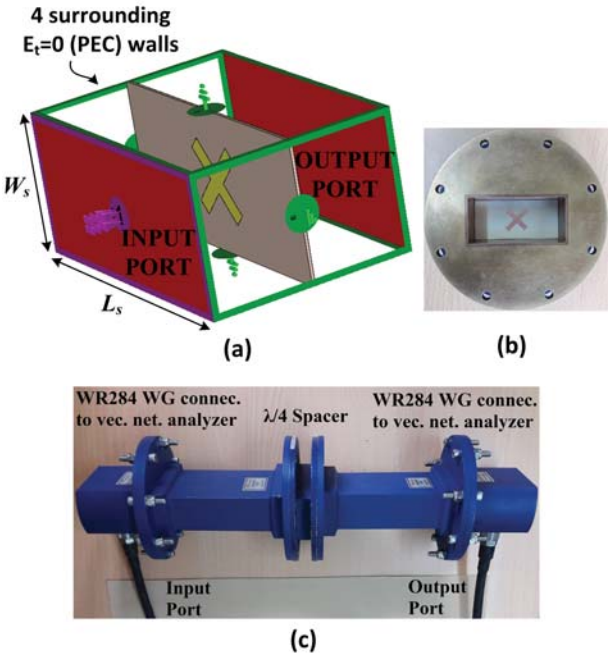

Figure 2: (a) The schematic views of the simulation setup. (b) The picture of λ/4 spacer with a sample prototype. (c) The photograph of the measurement setup.

3 Simulation and measurement results

Based on the design parameters and using the numerical and experimental setups, as explained in the previous section, the symmetrical and asymmetrical configurations of the proposed absorber have been simulated and measured. The simulated and measured absorptions characteristics have been computed using the following equation:

$$absorption = 1 - \left|S_{11}\right|^2 - \left|S_{21}\right|^2 \tag{3}$$

Where S_{11} and S_{21} parameters denote reflectance and transmittance, respectively, since the bottom face of the structure is completely covered with the ground plane, the transmittance is set as zero. Fig. 3(a) and (b) show the proposed design's simulated and measured absorption spectra for symmetrical and asymmetrical

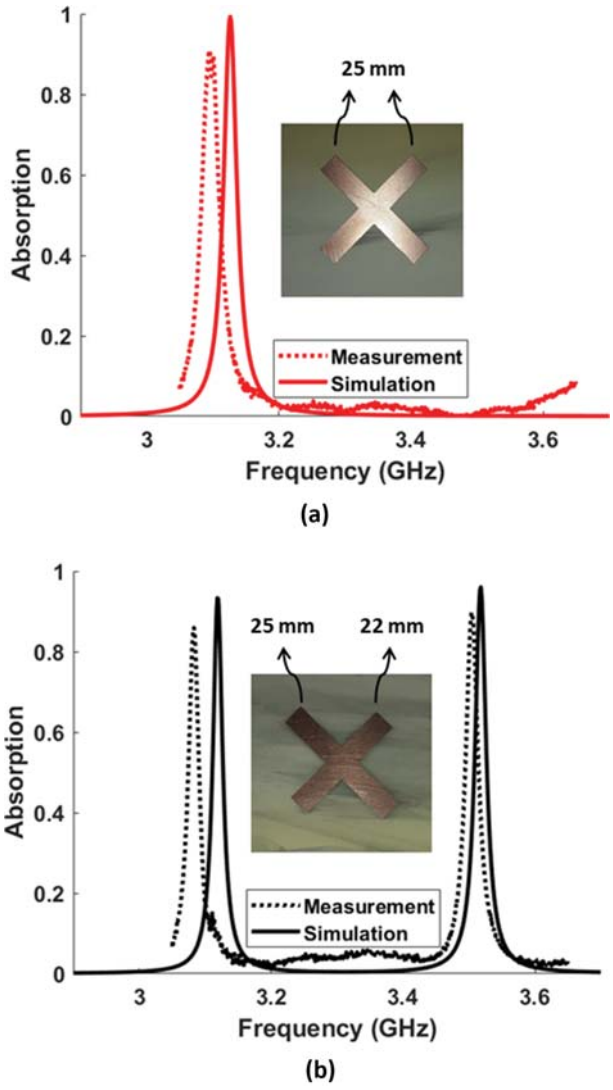

Figure 3: Simulation and measurement absorption characteristics for (a) symmetrical configuration and (b) unsymmetrical configuration.

configurations, respectively. As seen from the figures, the absorber with the symmetrical resonator ($l_1 = l_2$=25 mm) offers a single-band absorption peak at 3.13 GHz. On the other hand, the asymmetrical resonator (l_1=22, l_2=25 mm) provides dual-band absorption peaks at 3.12 GHz and 3.52 GHz. In addition, over 90% absorption peak levels are observed for all of the respective frequencies.

Since it is known that cross-polarized reflection can occur in asymmetrical structures, the cross-polarized reflection of the dual-band absorber has also been analyzed in this study. In this analysis process, as computation of the cross-polarized reflection is impossible in a rectangular waveguide, a free-space super-cell periodic array has been formed in the CST Studio Suite with two Floquet modes as reported in [22]. For applying the super-cell array, periodic boundary conditions (PBCs) have been imposed at the boundaries of a super-cell, as shown in Fig. 4(a). Also, the mirror image effect of the waveguide PEC walls has been taken into account in the simulator. As a result, the simulator has calculated co- and cross-polarized reflections for the free-space arrays. The absorption spectra have been computed using the formula (4) obtained from Reference [22].

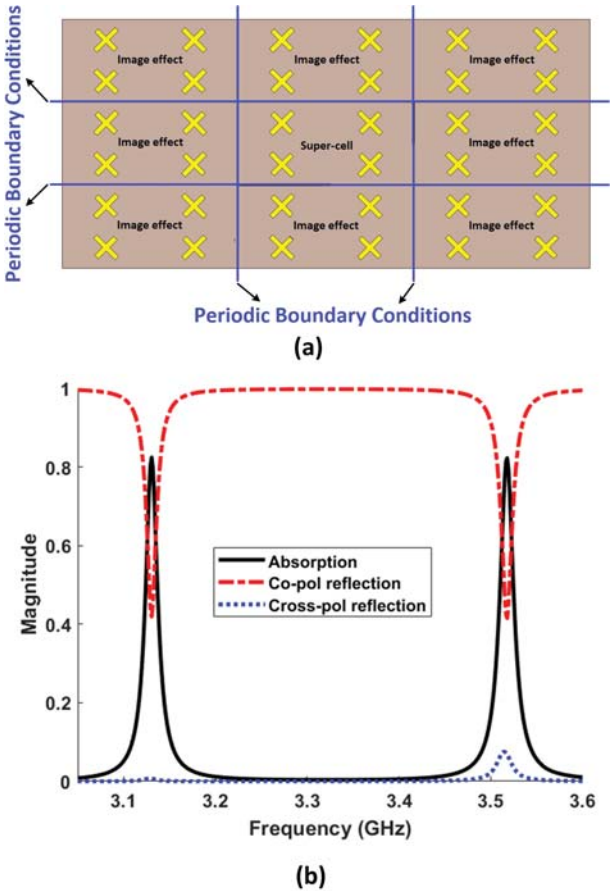

Figure 4: (a) Super-cell structure for dual-band absorber. (b) Absorption result regarding cross-polarized reflection, co- and cross-polarized reflections of dual-band absorber for the super-cell array.

$$absorption = 1 - \left|S_{11(co-)}\right|^2 - \left|S_{11(cross-)}\right|^2 \quad (4)$$

Herein, the transmittance is zero due to the presence of the metal ground plane of the absorber structure. According to the calculation, absorption levels of more than 0.8 can be achieved at both frequencies, as shown in Fig. 4(b).

Moreover, we have investigated the surface current density distributions at the related frequencies to support the proposed design's behavior. The simulated current density distributions on both resonator and ground plane of the proposed absorber design at the absorption peaks' frequencies are illustrated in Fig. 5(a) and 5(b), respectively. Herein, the surface currents on the XSR flow through the long arm at the lower frequency mode and flow through the shorter arm at the higher frequency mode. Those surface currents flow uniformly in the related arm of the resonator, and vertical surface currents at the edges of the corresponding arm exhibit the electric dipole resonance behavior. Also, the surface currents flowing at the ground plane in the opposite direction to the currents at the resonator reveal circulation current, which indicates the presence of magnetic dipole.

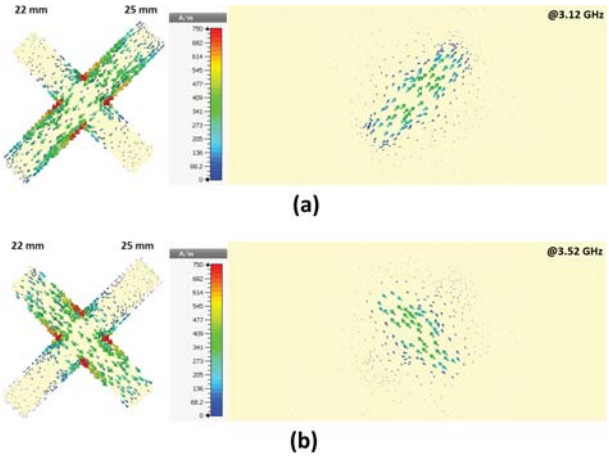

Figure 5: Surface current distributions on XSR and ground plane at 180° phase angle for (a) at 3.12 GHz and (b) at 3.52 GHz.

4 Sensing performance of the proposed absorber

The sensing performance of the XSA has also been investigated in this study for sensor applications. For this

purpose, the sensitivity of the change in the absorption frequency depending on the dielectric constant (ε_s) and thickness (h_s) variations of a dielectric material placed on the absorber and called the sensing layer has been observed numerically and experimentally. In addition, the same analyzes and measurements have been carried out for the SRRs designed in this study, and their sensing performances have been compared. A typical structure used for the sensitivity analysis of the XSA is shown in Fig. 6. Before presenting the numerical and experimental results obtained, the effect of the sensitivity layer on the absorption frequency is analyzed analytically, considering Fig. 6.

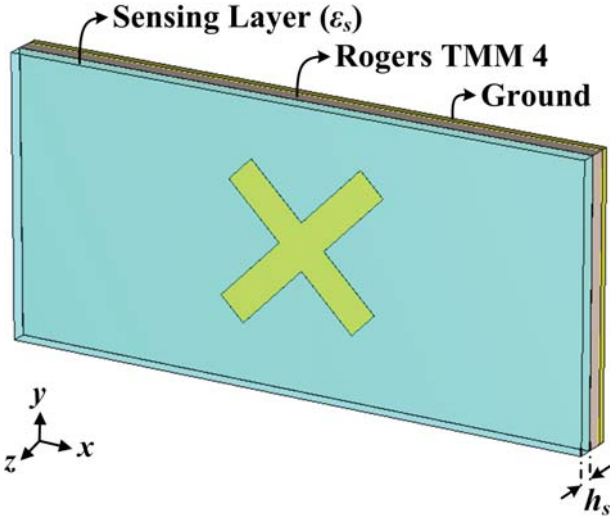

Figure 6: Schematic view of the absorber with the added sensing layer.

As known, the resonant frequency (f_0) can be defined as the following expression;

$$f_0 = \frac{1}{2\pi\sqrt{L_{Total}C_{Total}}} \tag{5}$$

Where L_{Total} and C_{Total} denote total inductance and capacitance of the structure, respectively. Since it is independent of the dielectric property and thickness of the sensing layer, the inductance value does not change [23]. The equivalent total capacitance of the structure consisting of three connected capacitors in series can be obtained using the equation (6). Herein, C_{Abs}, C_{Sen}, and C_{Air} represent the capacitance of the absorber, sensing layer, and air; also, their capacitances can be defined as in equations (7), (8), and (9), respectively. Herein, ε_r and ε_s represent permittivity of the absorber and sensing layer, while h and h_s denote their thickness.

$$\frac{1}{C_{Total}} = \frac{1}{C_{Abs}} + \frac{1}{C_{Sen}} + \frac{1}{C_{Air}} \tag{6}$$

$$C_{Abs} = \frac{\varepsilon_r \varepsilon_0 A}{h} \tag{7}$$

$$C_{Sen} = \frac{\varepsilon_S \varepsilon_0 A}{h_s} \tag{8}$$

$$C_{Air} = \frac{\varepsilon_0 A}{d - h_s} \tag{9}$$

Substituting (7-9) into (6), we can write the total equivalent capacitance as in (10), where d is the entire thickness of the air and sensitivity layer. Here, an air gap of an optimum thickness (d-h_s) is defined on the sensitivity layer for a more realistic calculation of the capacitance value. It is stated that this air gap is at least λ/4 in Electromagnetics Solver based on the finite element method [24]. In this context, the frequency range of the WR284 waveguide is 2.6 to 3.95 GHz. The quarter wavelength of 2.6 GHz of lower frequency is 28.85 mm, and the air gap thickness d is chosen at this value.

$$C_{Total} = \frac{\varepsilon_r \varepsilon_s \varepsilon_0 A}{\varepsilon_r h_s + \varepsilon_s h + \varepsilon_r \varepsilon_s \left(d - h_s\right)} \tag{10}$$

According to equation (10), as the dielectric constant and the thickness of the sensitivity layer increase, the total capacitance also increases, and thus the resonance frequency decreases.

4.1 Simulation and measurement results

To observe the sensing performance of the XSA, its dual-band configuration introduced in the previous section (see Fig. 3(b)) has been analyzed and measured again by placing different sensing layers on it. In these processes, copper-free pure dielectric Rogers RO3006 with the dielectric constant of 6.15 and RO3010 with the dielectric constant of 10.2 materials have been used as sensing layers. Also, the thicknesses of the materials are 0.64 and 1.28 mm.

Fig. 7 and 8 show the simulated and measured absorption characteristics for two different dielectrics constant (6.15 and 10.2) and thickness (0.64 and 1.28 mm) of the sensing layer, respectively. As seen, the simulation and measurement results are in perfect agreement except for slight frequency shifts, probably due to fabrication prototypes and measurement errors. The simulation and measurement results show that the absorber offers dual-band absorption at 3.12 and 3.52 GHz without a sensing layer with very narrow bandwidths. When the sensing layer's permittivity increases, the absorption frequencies shift to lower values, as shown in Fig. 7.

Similarly, when the thickness of the sensing layer is increased, the absorption frequencies move downward, as shown in Fig. 8.

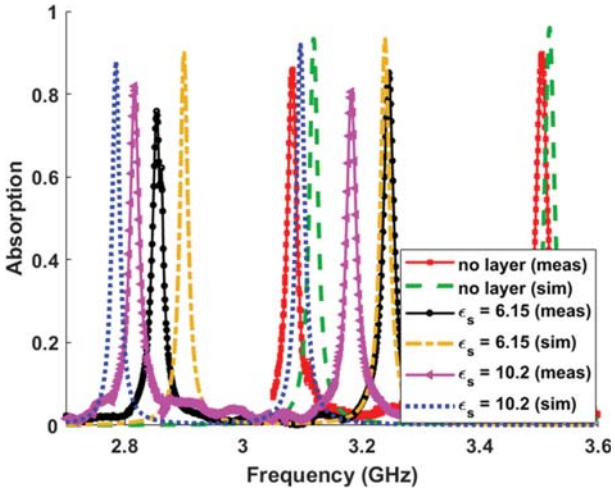

Figure 7: Simulation and measurement results for the different dielectric constant of the sensing layer with 0.64 mm thickness for dual-band absorber.

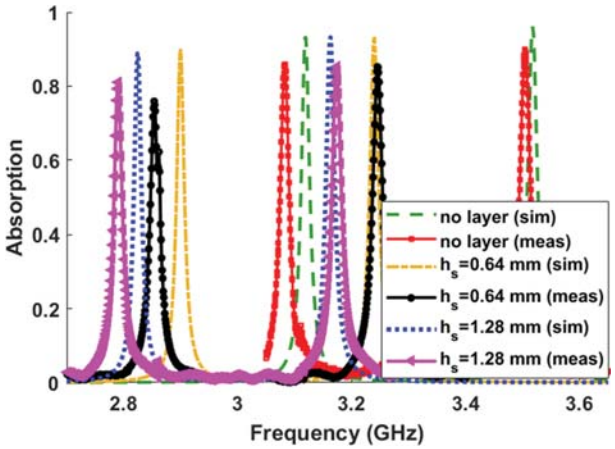

Figure 8: Simulation and measurement results for the different thicknesses of the sensing layer (h_s) with ε_s of 6.15 for the dual-band absorber.

4.2 Performance comparison of the X-shaped and the SRR-based absorbers

In this section, the sensing performance of the dual-band XSA is compared with two separate single-band SRRAs, namely SRR_{low} and SRR_{up} operate in the lower (3.12 GHz) and upper (3.52 GHz) bands of the XSA. Prototype fabrications of the absorbers designed in this study were also performed. Configuration, design parameters, a sample prototype, and configuration with sensing layer are depicted in Fig. 9. The analysis and measurements conducted for the XSA in the previous section are repeated for each SRRA, and the results are illustrated in Fig. 10. As seen from the simulation results in Fig. 10 (a) and (b), the SRR_{low} absorber operates at 3.12 GHz, and SRR_{up} operates at 3.52 GHz without sensing layers. On the other hand, when the permittivities of the sensing layer placed on the absorbers are increased, the absorption frequencies shift to the lower value for both SRRAs.

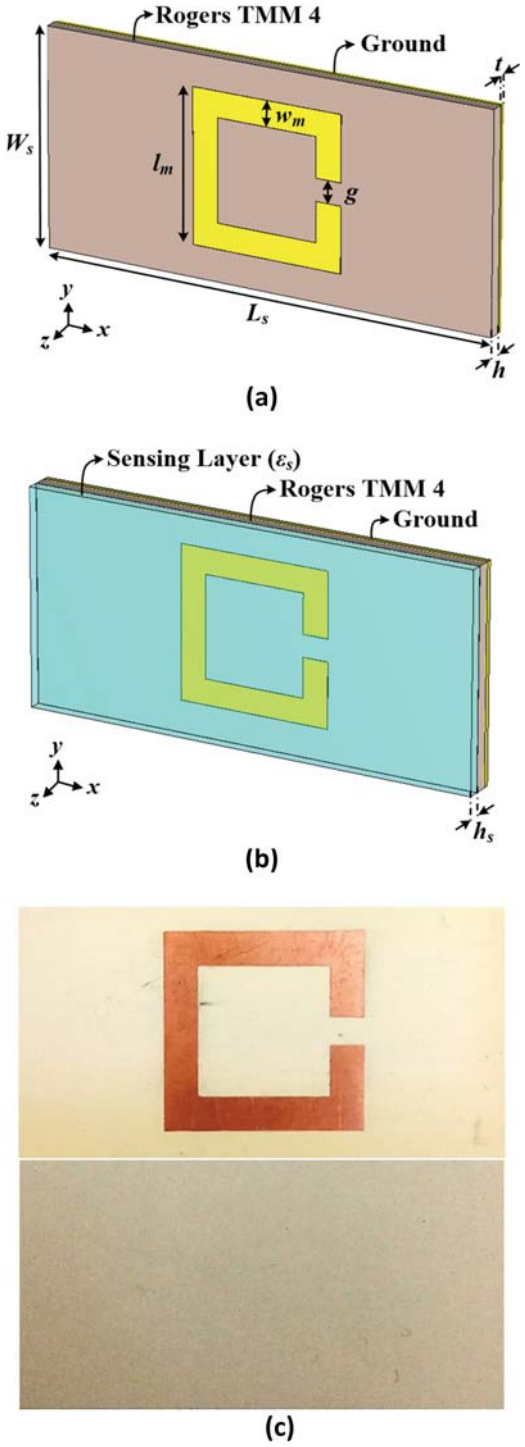

Figure 9: (a) The schematic views and design parameters of the SRRA (l_m=24, w_m=4 and g=3.5 for SRR_{low} and l_m=22, w_m=4 and g=4 for SRR_{up}, all in mm). (b) SRRA with sensing layer. (c) Prototype samples of the SRRA and sensing layer.

The simulated and measured absorption frequencies of the absorbers with and without the sensing layers are given in Table 1, comparatively. Herein, f_0 and f_s denote absorption frequencies without and with the sensing layer, respectively. The frequency shifts in the table are calculated using the following equation.

$$\%\, freq\ shift = \frac{f_0 - f_s}{f_0} \times 100 \tag{11}$$

Based on the frequency shift values given in the table, it is found that the sensing performance is higher in both frequency bands than SRRAs.

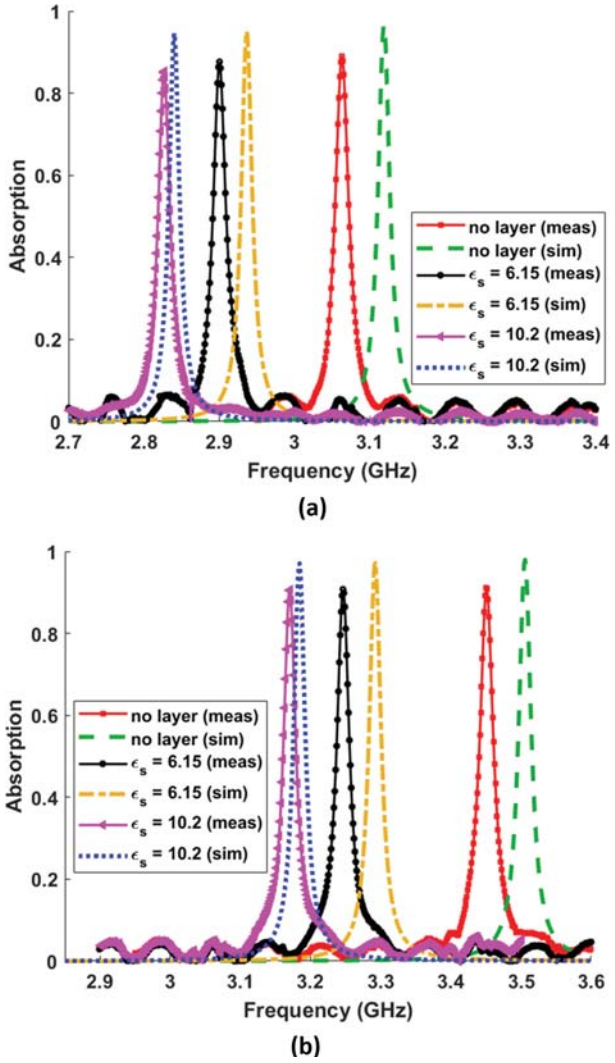

Figure 10: Simulation and measurement results for the different dielectric constant of the sensing layer for (a) SRR_{low} and (b) SRR_{up}.

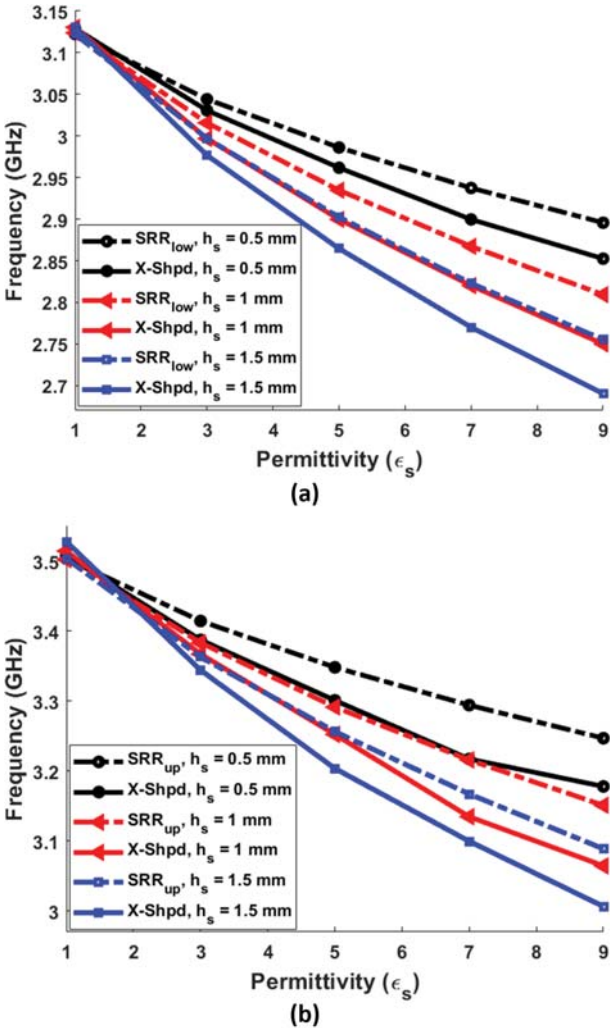

Figure 11: Characteristics of the change in the absorption frequency obtained in the simulation environment depending on various thickness (h_s) and dielectric constant (ε_s) values in the (a) lower band and (b) upper band.

Table 1: Numerical and experimental results for the proposed and SRRAs.

Structure	Sensing Layer	Simulation		Measurement	
		f_s (GHz)	freq shift (%)	f_s (GHz)	freq shift (%)
Proposed Absorber	No Layer	3.12 3.52	—	3.08 3.5	—
SRRlow		3.12	—	3.06	—
SRRup		3.52	—	3.45	—
Proposed Absorber	Rogers RO3006	2.90 3.24	7.05 7.95	2.85 3.25	7.47 7.14
SRRlow		2.94	5.80	2.90	5.23
SRRup		3.29	6.27	3.25	5.80
Proposed Absorber	Rogers RO3010	2.79 3.10	10.58 11.93	2.82 3.18	8.44 9.14
SRRlow		2.84	8.97	2.83	7.52
SRRup		3.19	9.12	3.17	8.12

In addition, for the proposed dual-band absorber and each SRRA, the change in the absorption frequency depending on five different dielectric constants and three different thickness values of the sensing layer have been computed in the simulation environment. The simulation results have been comparatively plotted in Fig. 11. It can be seen that the sensing performance of the proposed dual-band absorber is higher than the SRR_{low} in the first band (see Fig. 11 (a)) and the SRR_{up} in the second band (see Fig. 11 (b)) for all thickness and dielectric values of the sensing layer.

5 Conclusions

In this article, a novel absorber design based on an XSR has been introduced. The numerical and experimental results have shown the proposed design offers a single band performance for the case of the symmetrical conducting arms of the XSR and a dual-band operation for the asymmetrical resonator case. In addition, more than 90% of the absorption peaks and relatively narrow bandwidth characteristics have been achieved in the respective bands, as desired, especially for sensor applications. Moreover, It has been found the calculated values of the cross-polarized reflections at the relevant frequencies are smaller than 0.08. Besides, based on the simulated and measured results, it has been observed that the dual-band absorber is more sensitive in both bands than the SRRA designed in this study. On the other hand, by only scaling the design parameters of the proposed design, new absorber configurations exhibiting the same performance can be easily obtained for different frequency regions. Because of these prominent advantages, the proposed absorber structure is a good candidate for sensors and other microwave applications.

6 Acknowledgments

The authors acknowledge the Department of Electrical and Electronics Engineering, Suleyman Demirel University, for providing us the opportunity for the absorber S-parameter measurements in vector network analyzer. And also, the authors would like to thank Assoc.Prof. Dr. Evren Ekmekci, N. Karacan, K.C. Ayvaci, B. Ila, and N.K. Bulut for their help.

7 Conflict of interest

We declare that we do not have any commercial or associative interest that represents a conflict of interest in connection with the work submitted.

8 References

1. N. I. Landy, S. Sajuyigbe, J. J. Mock, D. R. Smith and W. J. Padilla, "A Perfect Metamaterial Absorber", *Phys Rev Lett*, vol. 100, no. 20, pp. 207402, 2008. https://doi.org/10.1103/PhysRevLett.100.207402
2. E. Unal, F. Dincer, E. Tetik, M. Karaaslan, M. Bakir, and C. Sabah, "Tunable perfect metamaterial absorber design using the golden ratio and energy harvesting and sensor applications", *J Mater Sci Mater El*, vol. 26, no.12, pp. 9735-9740, 2015. https://doi.org/10.1007/s10854-015-3642-7
3. K. S. Al-Badri, A. Cinar, U. Kose, O. Ertan, and E. Ekmekci, "Monochromatic tuning of absorption strength based on angle-dependent closed-ring resonator-type metamaterial absorber", *IEEE Antennas Wirel Propag Lett*, vol. 16, pp. 1060-1063, 2016. https://doi.org/10.1109/LAWP.2016.2620599
4. E. Ekmekci, and E. Demir, "On/off switching of absorption spectra by layer shifting for double-layer metamaterial-based absorber", *IEEE Antennas Wirel Propag Lett*, vol. 15, pp. 532-535, 2015. https://doi.org/10.1109/LAWP.2015.2457091
5. K. Ozden, O. M. Yucedag, and H. Kocer, "Metamaterial based broadband RF absorber at X-band", *AEU-Int J Electron C*, vol. 70, no. 8, pp. 1062-1070, 2016. https://doi.org/10.1016/j.aeue.2016.05.002
6. S. Li, X Cao, T. Liu, and H. Yang, "Double-layer perfect metamaterial absorber and its application for RCS reduction of antenna", *Radioengineering*, vol. 23, no. 1, pp. 222-229, 2014. radioeng.cz/papers/2014-1.htm
7. H. Wang, and L. Wang, "Perfect selective metamaterial solar absorbers", *Opt Express*, vol. 21, no. 106, pp. A1078-A1093, 2013. https://doi.org/10.1364/OE.21.0A1078
8. N. Mishra, K. Kumari, and R. K. Chaudhary, "An ultra-thin polarization-independent quad-band microwave absorber based on compact metamaterial structures for EMI/EMC applications", *Int J Microw Wirel T*, vol. 10, no. 4, pp. 422-429, 2018. https://doi.org/10.1017/S1759078718000491
9. A. Hoque, M. Tariqul Islam, A. F. Almutairi, T. Alam, M. Jit Singh, and N. A. Amin, "A polarization-independent quasi-TEM metamaterial absorber for X and Ku band sensing applications", *Sensors*, vol. 18, no. 12, pp. 4209, 2018. https://doi.org/10.3390/s18124209
10. M. Bakir, M. Karaaslan, O. Akgol, O. Altintas, E. Unal and C. Sabah, "Sensory applications of resonator-based metamaterial absorber", *Optik,* vol. 168, pp. 741-746, 2018. https://doi.org/10.1016/j.ijleo.2018.05.002

11. M. Bakır, M. Karaaslan, E. Unal, O. Akgol, and C. Sabah, "Microwave metamaterial absorber for sensing applications", *Opto-Electron Rev*, vol. 25, no. 4, pp. 318-325, 2017. https://doi.org/10.1016/j.opelre.2017.10.002
12. M. L. Hakim, T. Alam, A. F. Almutairi, M. F. Mansor, and M. T. Islam, "Polarization insensitivity characterization of a dual-band perfect metamaterial absorber for K band sensing applications", *Sci Rep*, vol. 11, no. 1, pp. 1-14, 2021. https://doi.org/10.1038/s41598-021-97395-0
13. A. Abdelsallam, A. Gaafar, and M. Abdalla, "Oblique and Polarization Independent Metasurface-Based Absorber for Bio-Sensing Applications", *IETE J Res*, pp. 1-10, 2021. https://doi.org/10.1080/03772063.2021.1920853
14. X. Ling, Z. Xiao, and X. Zheng, "Tunable terahertz metamaterial absorber and the sensing application", *J Mater Sci: Mater Electron*, vol. 29, no. 2, pp. 1497-1503, 2018. https://doi.org/10.1007/s10854-017-8058-0
15. M. R. Nickpay, M. Dannie, and A. Shahzadi, "Highly sensitive THz refractive index sensor based on folded split-ring metamaterial graphene resonators", *Plasmonics*, pp. 1-12, 2021. https://doi.org/10.1007/s11468-021-01512-8
16. M. S. Sim, K. Y. You, F. Esa, M. N. Dimon, and N. H. Khamis, "Multiband metamaterial microwave absorbers using split ring and multi-width slot structure", *Int J RF Microwave Comput Aided Eng*, vol. 28, no. 7, pp. e21473, 2018. https://doi.org/10.1002/mmce.21473
17. M. A. Shukoor, V. Kumar, and S. Dey, "Compact polarisation insensitive wide angular stable triple-band absorber for RF energy harvesting, RCS reduction, and sensor applications", *Int J RF Microwave Comput Aided Eng*, vol. 31, no. 9, pp. e22763, 2021. https://doi.org/10.1002/mmce.22763
18. Y. I. Abdulkarim, L. Deng, O. Altıntaş, E. Ünal, and M. Karaaslan, "Metamaterial absorber sensor design by incorporating swastika-shaped resonator to the determination of the liquid chemicals depending on electrical characteristics", *Physica E*, vol. 114, pp. 113593, 2019. https://doi.org/10.1016/j.physe.2019.113593
19. A. Hoque, M. T. Islam, A. F. Almutairi, M. E. H. Chowdhury, and Md. Samsuzzaman, "SNG and DNG meta-absorber with fractional absorption band for sensing application", *Sci Rep*, vol. 10, no.1, pp. 1-17, 2020. https://doi.org/10.1038/s41598-020-69792-4
20. M. Amiri, M. Abolhasan, N. Shariati and J. Lipman, "Soil moisture remote sensing using SIW cavity-based metamaterial perfect absorber", *Sci Rep*, vol. 11, no.1, pp. 1-17, 2021. https://doi.org/10.1038/s41598-021-86194-2
21. D. M. Pozar, "Microwave Resonators," in Microwave Engineering, 4th ed. Hoboken, United States of America: John Wiley & Sons, Inc., 2012, ch. 6, sec. 2, pp. 283.
22. N. Karacan, E. Ekmekci, and G. Sayan, "Response to "Comment on 'Sliding planar conjoined cut-wire-pairs: A novel approach for splitting and controlling the absorption spectra'" [J. Appl. Phys. 128, 126101 (2020)]", *J Appl Phys*, vol. 128, pp. 126102, 2020. https://doi.org/10.1063/5.0018386
23. E. Ekmekci, and G. Turhan-Sayan, "Multi-functional metamaterial sensor based on a broad-side coupled SRR topology with a multi-layer substrate", *Appl Phys A*, vol. 110, no. 1, pp. 189-197, 2013. https://doi.org/10.1007/s00339-012-7113-1
24. O. E. Mrabet, "High frequency structure simulator (HFSS) tutorial", *IETR UMR CNRS 6164*, 2006.

Arrived: 14. 02. 2022
Accepted: 12. 07. 2022